Progress In Electromagnetics Research, Vol. 146, 195–207, 2014

Miniaturized Low Frequency Platform Tolerant Antenna

Shaozhen Zhu[1], Daniel Graham Holtby[2], Kenneth Lee Ford[3, *], Alan Tennant[3], and Richard J. Langley[3]

Abstract—A miniature platform tolerant antenna is presented which is suitable for low frequency applications. A Split Ring Resonator (SRR) antenna loaded with lumped capacitances is proposed, and the antenna is compact, low profile and easy to fabricate. It has a maximum dimension of $\lambda/9$ and -10 dB bandwidth of 1%. Miniaturized artificial magnetic conductor surfaces (AMCs) are designed using capacitance loaded metal patches with individual elements measuring just $\lambda/70$. Placing the SRR above the AMC improves the bandwidth to between 1.5 and 3.5% dependent on the overall size of the AMC and produces a platform tolerant antenna measuring $0.11\lambda \times 0.17\lambda \times 0.019\lambda$. The performance of the antenna over an AMC with and without vias is studied and discussed. The AMC mounted antenna performances in free space and over a ground plane are also compared.

1. INTRODUCTION

The design of Electrically Small Antennas (ESAs) is a topic of considerable interest within the antenna community. Of particular interest is the design of miniaturized antennas which operate at low frequencies, as traditional approaches to antenna design result in large and bulky structures. Electrically small antennas are well known to be inefficient radiators because of their very small radiation resistance. Consequently it is very difficult to match these antennas to any realistic power source and results in very narrow bandwidth and poor efficiency. The well-known Chu limit [1–3] defines the fundamental limits on the radiation quality factor, Q, associated with electrically small antennas. The minimum quality factor is defined as

$$Q_{chu} = \frac{1}{(ka)^3} + \frac{1}{ka} \tag{1}$$

where a is the radius of the minimum radius sphere of the antenna and $k = 2\pi/\lambda$ the wave number for corresponding operational frequency. If the antenna efficiency utilizes the available volume within the radiation sphere, the gain approaches the maximum limit and equals the normal directivity:

$$G_{\max} = D = (ka)^2 + 2ka \tag{2}$$

The fractional bandwidth of the antenna system is inversely proportional to the quality factor Q. For an ESA, because of its compact size, it is very likely to have a high Q value and consequently narrow bandwidth and poor gain and efficiency. Therefore, there is a real challenge to design ESAs with high overall radiation efficiency and broad bandwidth. Various approaches to antenna miniaturization have been investigated, including the use of high permittivity materials and substrates [4]; electrically loading antennas with reactive components [5, 6]; antennas which utilize the properties of metamaterial structures [7–11] and composite right/left handed transmission line based resonant antennas [12–15].

There has also been much interest in producing platform tolerant antennas which can be used on automobiles, aircraft, etc. Integrating numerous antennas into these platforms can be challenging,

Received 3 April 2014, Accepted 17 May 2014, Scheduled 11 June 2014

* Corresponding author: Kenneth Lee Ford (l.ford@sheffield.ac.uk).

[1] Seven Technologies Group, 1 Low Hall Business Park, Horsforth, Leeds LS18 4EG, UK. [2] Department of Automatic Control and Systems Engineering, University of Sheffield, UK. [3] Department of Electronic and Electrical Engineering, University of Sheffield, UK.

because of limited space, cost and electromagnetic interference issues. Therefore, to reduce the conventional antenna size and provide platform tolerance properties is an important objective for such applications. One of the solutions is achieved by combining antennas with high impedance surfaces or Artificial Magnetic Conductors (AMCs) [16–19]. Electromagnetic Band-gap Materials (EBGs) and AMCs have been found to have two main attractive attributes: as surface wave suppressors and high impedance surfaces. Application areas for such surfaces include antenna miniaturization, impedance bandwidth improvement and radiation pattern control. Traditionally AMCs are based on designs in which the size of the element unit cell is typically of the order of $\lambda/3$. The size limitation has an impact on practical AMC design at low frequencies. However, by using modified cell geometries which are loaded with lumped element components, the authors have demonstrated that the cell dimensions can be reduced to $\lambda/50$ or smaller [20, 21].

In this paper, we present details of the design of a novel compact split ring resonator antenna which is integrated with a miniaturized AMC. Both the antenna and the AMC utilize loading by discrete, lumped circuit elements to significantly reduce the size of the overall radiating structure. To further miniaturize the AMC, its effectiveness as a platform tolerant surface is evaluated as both the number of unit cells and their periodicity are decreased. The antenna and the AMC were both designed with the aid of the CST Microwave Studio software suite. The results of numerical simulations of the antenna performance with regard to input match and radiation patterns are presented and compared to measured data.

2. ANTENNA DESIGN AND MINIATURIZATION

SRRs were found to have negative permeability features [22, 23] that can generate a resonance at wavelengths much larger than their own electrical dimensions in a certain frequency range. The equivalent circuit model of a double-ring SRR is shown in Fig. 1. The individual outer ring and inner ring are simple RLC resonators with resonant frequency $\omega_0 = 1/\sqrt{LC}$. The double-ring configuration adds a coupling capacitance C_m and a higher current density and therefore produces a larger magnetic affect generating a lower resonant frequency.

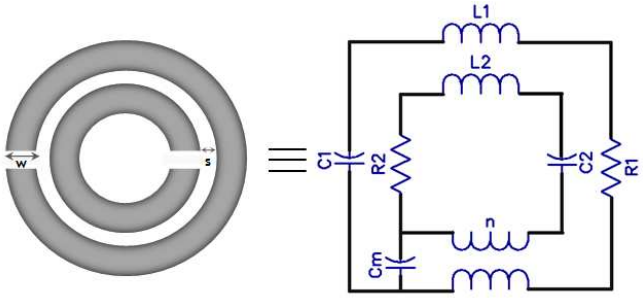

Figure 1. Equivalent circuit model of a double-ring SRR.

Previous applications of SRRs mainly used split rings to form Frequency Selective Surfaces (FSSs) [24], or using SRRs as parasitic elements to affect the resonance of an existing antenna [11]. In this paper, we present an electrically small antenna which uses SRRs as the main radiating elements. In addition, lumped circuit elements are used to realize further miniaturization of the antenna.

The split ring dipole geometry is shown in Fig. 2. It is composed of two split ring resonators (SRR) forming a dipole as the main radiating element. The two identical SRRs are printed symmetrically on opposite sides of the substrate to form the dipole arms. The resonance of the structure is due to the resonance of the SRRs. For a double-ring configuration SRR, the capacitive coupling and inductive coupling between the larger and smaller rings are vital to define the resonant frequency. A larger coupling capacitance will further reduce the resonant frequency. Therefore, to realize the miniaturization of the antenna, two lumped capacitors are loaded in between the inner and outer rings of the SRR, symmetrically at the top and bottom of the split rings as shown in Fig. 2. The resonance of the antenna can be tuned by simply varying the value of the capacitance.

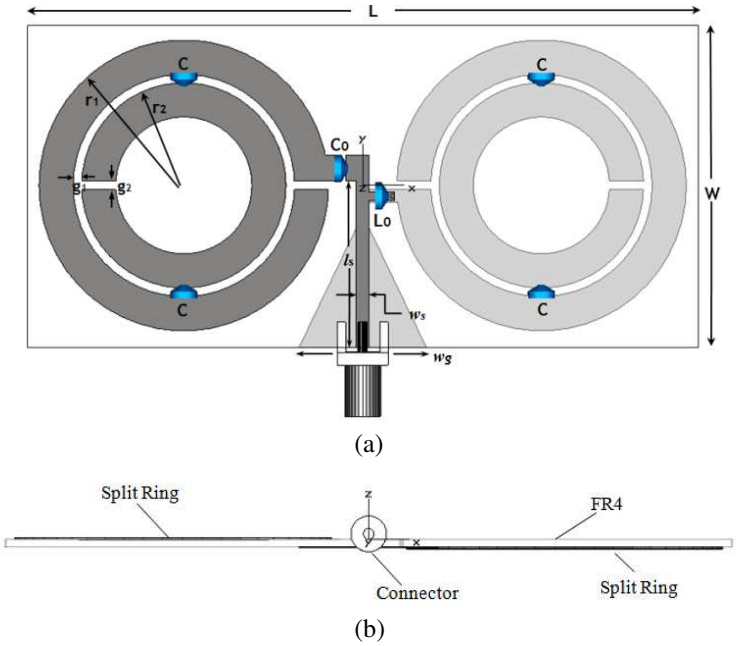

Figure 2. Split ring resonator antenna geometry. (a) Top view. (b) Side view.

The antenna is fed by a microstrip line over a tapered ground plane via a simple LC matching network. The LC matching network which consists of a series capacitor and a parallel inductor connecting the bottom element is used to enhance the impedance matching of the resonances, and it also helps to balance the current at the SMA connector. The proposed SRR antenna is fabricated on FR4 substrate with a dielectric constant of 4.5 and thickness of 0.8 mm. A series capacitance value of $C_0 = 18$ pF and shunt inductance value of $L_0 = 15$ nH are chosen as shown in Fig. 2. The resonant frequency is mainly defined by the ring radius and the capacitive coupling between the rings. The width of the split ring and the gap between the inner and outer rings can be tuned to achieve the best match at the resonance in this antenna design. Thus, the proposed antenna provides the features of easy fabrication and a low profile. The antenna's dimensions are in mm, $L = 78$, $W = 38$, $r_1 = 17$, $r_2 = 12$, $g_1 = g_2 = 1$, strip line length $l_s = 19.5$, width $w_s = 1.5$, and tapered ground width at the terminal $w_g = 15$. The loading capacitance value is the main factor that tunes the resonant frequency in this antenna design. For the 4 pF capacitance value used in this example the antenna has a resonant frequency of around 446 MHz. A SRR dipole without any capacitance loading is approximately 25% larger. The antenna has an overall size of 78 mm by 38 mm by 0.8 mm ($ka = 0.36$), which at the free space operating wavelength at 446 MHz measured $\lambda/9 \times \lambda/18 \times \lambda/838$.

Figure 3 shows the simulated and measured reflection coefficients of the SRR antenna with a 4 pF loaded capacitance. Simulated reflectivities of the antenna with and without the LC matching circuit are also compared. It can be seen that without the LC matching circuit, the antenna is not well matched at the resonant frequency due to the very low radiation resistance. The impedance matching can be improved significantly by simply inserting a shunt capacitor and a series inductor at the feeding strip line. Measurements were carried out not only with the matching network but also with an external magnetic choke cable which stops the unbalanced current radiating from the coaxial cable. A 1% -10 dB impedance bandwidth was achieved at 443 MHz in the measurement, which is good for such a small antenna.

Figure 4 shows the simulated current distribution on the antenna at the resonant frequency. It can be seen that the surface currents are mainly induced by the driven ring itself and the large capacitances in between the split rings which are introduced by the load capacitors. The measured radiation patterns of the SRR antenna at its resonant frequency are plotted in Fig. 5, and the measured realized gain of the antenna was -1.2 dBi. The antenna has dipole-like radiation patterns, omnidirectional in the H-plane and a figure of eight in the E-plane. The cross polarization levels are approximately -15 dB.

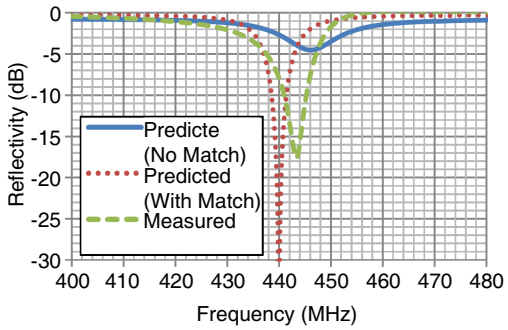

Figure 3. Loaded SRR antenna reflectivity ($c = 4\,\text{pF}$).

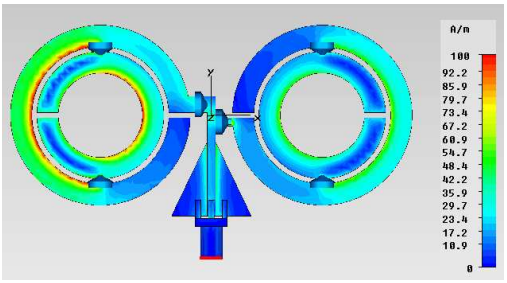

Figure 4. Simulated current distribution at the resonant frequency.

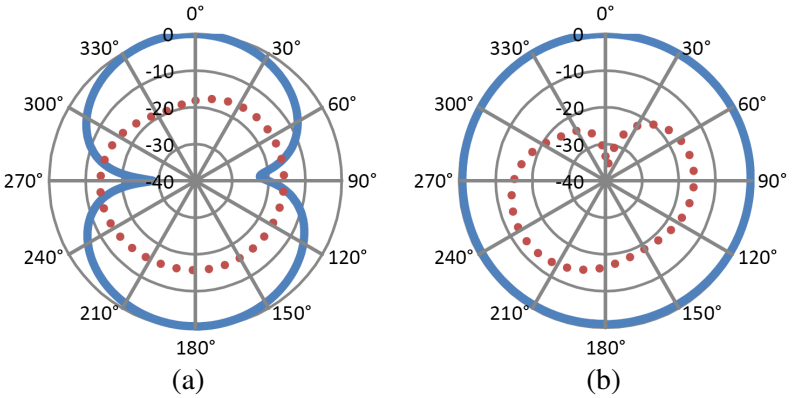

Figure 5. Measured co-polar (solid) and cross-polar (dotted) antenna radiation patterns normalized in the (a) E and (b) H plane.

3. AMC MINIATURIZATION

The square patch AMC is one of the most common and simplest AMC structures as it is low cost and easy to design. Classic AMC design uses periodic metallic elements to provide distributed capacitive or inductive properties, and the size of the element unit cell is typically of the order of $\lambda/3$. The miniaturized AMC [20] uses lumped capacitance components to provide the required reactance while the metallic elements are only there to provide a current path. The resonant frequency can be tuned by simply varying the capacitance value. In this research, we found that the unit cell size can be reduced to at least $\lambda/70$.

Figure 6 illustrates the loaded AMC unit cell surface, which is printed on a FR4 substrate of thickness h from a perfect electrical conductor ground plane. The AMC surface, whose periodicity is p, has a square patch of width d and capacitor C_0 at the centre of each edge connecting the neighboring cells. There are no vias. In this case the input admittance of the AMC is generally described by

$$Y_{in} = Y_c - \frac{jY}{\tan(\beta h)} \tag{3}$$

where Yc is the admittance of the front surface, Y the characteristic admittance of the substrate, and β the propagation constant in the substrate.

In this study, the simulations were carried out using unit cell boundaries to approximate an infinite structure in CST Microwave Studio. A square patch unit cell was created with four capacitors, one at the center of the each edge, to connect the neighboring patches. It was found that a thicker substrate will increase the bandwidth. However, in order to provide a very thin conformal surface while providing sufficient bandwidth, a 6.4 mm thick FR4 substrate was chosen in all of the AMC studies. Conducting vias were later added to observe the performance of the surface when acting as a high impedance plane,

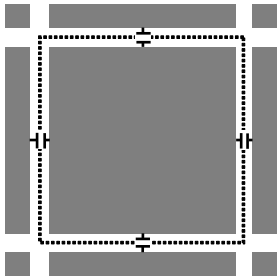

Figure 6. AMC unit cell geometry.

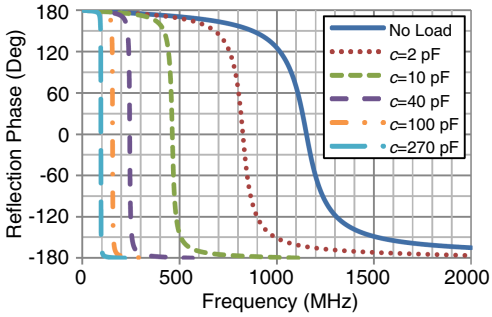

Figure 7. AMC reflection phase with various capacitive loading (unit cell size $p = 40$ mm).

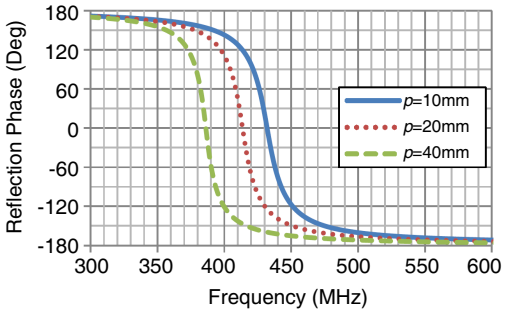

Figure 8. AMC reflection phase with various unit cell size (loaded $c = 15$ pF).

simulations of the reflection phase found no major differences with the presence of the vias. Adding the vias provides TE and TM surface wave suppression which is important for the miniaturization of the surface, this is discussed in Section 4.

At this stage, the miniaturization factor of the AMC cell was observed by either varying the load capacitance or modifying the patch size. First the AMC periodicity was fixed to 40 mm, with a square patch of width 39 mm and a 1 mm gap between adjacent unit cells. The simulated reflection phase of the surface was observed with no capacitor loading, and the results are shown in Fig. 7. It can be seen that without reactive loading, the zero degree phase reflection frequency occurred at 1150 MHz. When a 2 pF capacitance was loaded to the AMC surface, the in-phase reflection frequency dropped to 825 MHz. On increasing the capacitance to 10 pF, 40 pF and 100 pF, the corresponding frequencies were at 462 MHz, 243 MHz and 155 MHz. When a capacitance of 270 pF was used, the zero degree frequency dropped to 95 MHz, and the operational frequency decreased by about 90%. The unit cell size is now reduced to $\lambda/75$ which is a very significant miniaturization for low frequency designs.

The AMC performance was also studied by fixing the load capacitance value and varying the unit cell size. A 15 pF capacitance was loaded with three different AMC periodicities of 40 mm, 20 mm and 10 mm. The simulated reflection phase diagram is shown in Fig. 8. It can be seen that the zero degree reflection frequency shifted downward with the increasing periodicity. The 10 mm periodicity AMC had a resonant frequency of 432 MHz, doubling the periodicity gave a 4.2% shift in resonant frequency (414 MHz), and again to 40 mm, the resonant frequency dropped to 386 MHz, a reduction of approximately 6.8%. Hence the AMC miniaturization is easy to realize by simply increasing the reactive loading, and the unit cell size is not the main factor dominating the resonant frequency.

4. ANTENNA OVER AMC SURFACE

The miniaturized SRR antenna was integrated over the AMC to achieve a conformal antenna structure. Both simulations and measurements were carried out to verify the performance of the combined structure. Different AMC periodicities and numbers of elements were evaluated to determine the miniaturization limitation of the structure.

4.1. Simulation

The proposed SRR antenna in Fig. 2 was placed over six different AMC surfaces. The six AMC surfaces have three different periodicities, 40 mm, 20 mm and 10 mm. For each periodicity two different array sizes were studied as listed in Table 1. For all six surfaces, the performance with and without vias was also studied. Therefore, there were twelve antenna and AMC combined structures overall. The dimensions for each structure in terms of AMC unit cell periodicity and overall size are listed in Table 1. The load capacitance was chosen from the available values of the commercial surface mount products that can also achieve the AMC zero reflection phase close to the resonant frequency of the antenna. Therefore, the load capacitance values were set to 11 pF, 13 pF and 15 pF for the AMC periodicities of 40 mm, 20 mm and 10 mm, respectively. The simulated $-90°$ to $+90°$ reflection phase bandwidths of the three periodicity AMCs were 3.8% (434–451 MHz), 4.8% (432–453 MHz) and 4.8% (422–443 MHz), respectively. The space between the antenna and the AMC was set to be 6 mm in order to keep the thickness of the structure small but also be able to achieve an optimum impedance matching bandwidth for the antenna. The overall thickness was 13.2 mm for all cases which is 1/50 of the wavelength at the resonant frequency of 440 MHz.

Table 1. Simulation summary and comparison results for proposed structures.

AMC Periodicity		**40 mm**		**20 mm**		**10 mm**	
Size (mm × mm)		200×280	160×240	160×240	100×140	100×140	80×120
−10 dB Fractional Bandwidth (%)	**No Via**	1.2	1.1	0.6	0.7	0.6	0.5
	With Via	2.1	1.7	2.2	1.0	0.6	0.6
Realized Gain (dBi)	**No Via**	−9.4	−13.2	−14.5	−17.3	−18.5	−18.4
	With Via	−0.4	−2.1	2.1	−2.5	−1.4	−2.0

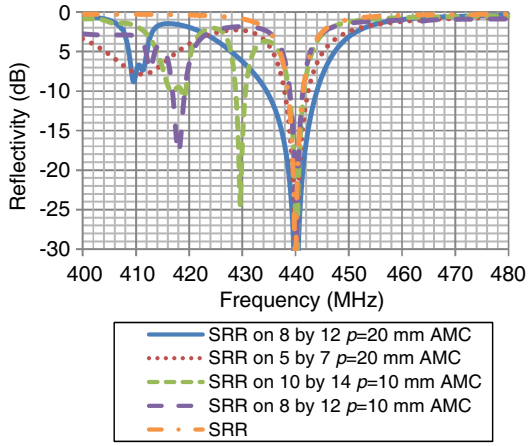

Figure 9. Simulated reflectivity of AMC mounted SRR.

The simulated antenna bandwidth and gain for the twelve different antenna and AMC combination structures are summarized in Table 1. All antenna and AMC configurations benefit from including vias with significant increases in the bandwidth and gain of the antennas which suggests that EBG surface wave suppression is of key importance for small cell sizes. It is also clear that the larger surfaces with more elements have a better performance, but reducing the overall size and hence element numbers still gives acceptable performance for all periodicities studied. Our simulation also suggests that the miniaturization of the AMC unit cell with vias can be further reduced to 5 mm ($\lambda/140$). However, the simulated performance deteriorated, and the details are not discussed here. Fig. 9 shows the

predicted reflection coefficient of the simulated SRR and AMC configurations with vias. In each case, the SRR matching network was adjusted to match the input impedance of the antenna at 440 MHz. The additional resonances of the radiating structures are caused by surface waves propagating across the finite surface and are therefore dependent on its overall size [25]. The radiation efficiency of the additional resonances were typically less than 10%. In all cases the radiation was at a maximum in the boresight direction, at 440 MHz.

Table 2 summarizes the effect of each loss mechanism on the radiation efficiency of an AMC mounted SRR. For the negligible loss condition, the metal tracks were modeled as a PEC, and the loss tangent of the substrate was set to 0.0001. For the dielectric and copper loss conditions, the loss tangent of the FR4 substrate was increased to 0.025, and all the PEC materials were replaced with copper. The component loss was introduced to the model by adding a 0.05 Ω series resistance to each capacitor and a 0.65 Ω series resistance to the inductor in the matching network. It can be seen that the major sources of loss are due to the relatively high loss tangent of the FR4 substrate and the conductivity of the copper tracks. In [11] and [26–30], the present ESA designs for use at comparable frequencies exhibit radiation efficiencies of roughly between 70–90%. In each case, however, the antenna is fabricated on Rogers Duroid 5880 ($\varepsilon_r = 2.2$, loss tan = 0.0009), with the exception of [30] which uses DuPont 951 ($\varepsilon_r = 7.8$, loss tan = 0.0015). Both our antenna and AMC have been fabricated on standard FR-4 ($\varepsilon_r = 4.3$, loss tan = 0.025) and consequently have a higher loss. If both the antenna and 8×12 20 mm periodicity AMC are constructed on a relatively loss-free substrate such as Duroid, the efficiency of the structure is predicted to be around 80%, which is more in line with those values reported by others. An electrically small spherical helix antenna is presented in [31], which boasts efficiencies of 90% plus; however, the antenna is mounted over an infinite Perfect Electric Conductor (PEC) ground plane and as such cannot truly be considered an ESA.

Table 2. Simulated radiation efficiency under different material conditions.

Material Loss Condition	**SRR on 8×12 $p = 20$ mm AMC**	**SRR on 8×12 $p = 10$ mm AMC**	**SRR Antenna**
Negligible Loss	88.5%	87.3%	98.6%
Dielectric Loss	74.7%	66.1%	20.2%
Copper Loss	81.2%	63.4%	44.0%
Dielectric & Copper Loss	68.4%	50.0%	16.1%
Dielectric & Copper & Component Loss	64.4%	37.5%	13.6%

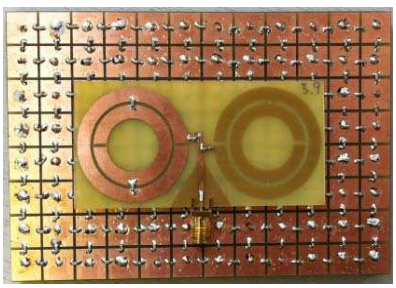

Figure 10. SRR antenna over 8 by 12 AMC surface ($p = 10$ mm), overall size 80 mm by 120 mm by 13.2 mm, $ka = 0.53$.

4.2. Measurement

To validate the simulation data, the AMC boards with and without vias were fabricated and tested with the SRR antenna. The antenna was placed 6 mm above the AMC using Rohacell foam which has a permittivity ($\varepsilon_r = 1.006$). Fig. 10 shows an example. All twelve AMC boards were tested, and the results agree well with the trend summarized from the simulation results. Here only the details of the measured results of the 10 mm and 20 mm periodicity AMC cells with vias are presented. A performance summary and comparison of the measured SRR antenna and the antenna with four AMC surfaces with vias are listed in Table 3. The antenna radiation efficiency was measured using the Wheeler Cap method [32]. Gains were measured against a standard folded dipole (420–470 MHz) which has a gain of 2.1 dBi. The SRR antenna only has a maximum radiation efficiency of 24% at around 440 MHz, which is slightly better than that predicted by our CST simulation result. By integrating with the AMC surfaces, the antenna gain and efficiency can be significantly improved. As the AMC becomes larger, the efficiency of the mounted antenna is improved because the radiating surface is larger. The maximum efficiency of the entire structure is 62%, which is relatively good considering the material loss and large number of surface mount elements. The simulated and measured gains agree within 1 dB.

The measured antenna reflection coefficients in free space are plotted in Fig. 11(a) for the antenna alone, and the antenna integrated over each AMC. The SRR antenna and integrated structures were also measured over a large metal plate to test the platform tolerance ability of the antenna/AMC structure. The SRR antenna was spaced the same distance of 13 mm away from the metal plate to make a direct comparison with the integrated structures. The large metal plate was circular and had a diameter of 0.9 m, about 1.3 times the free space wavelength at the resonant frequency.

From Fig. 11(a), we can see that in free space, the measured reflectivity of the structures match the simulated results very well. The antenna alone and all the integrated antenna/AMC integrated structures are well matched at around 440 MHz. However, compared to the antenna on its own, the AMC surfaces have significantly increased the bandwidth over which the antenna exhibits a return loss of better than −10 dB. For the 5×7 surface with a periodicity of 20 mm, the measured −10 dB frequency band is covered from 432 MHz to 448 MHz (3.6% at 444 MHz). From Fig. 11(b) it can be seen that when the antennas were placed above a large metal plate, the resonant frequency of the smaller combined structures were increased by around 10 MHz. Conversely, the return loss null of the antenna

Table 3. Measurement summary and comparison results for proposed structures with vias in free space and (on a groundplane).

	SRR on 8×12 $p = 20$ mm AMC	**SRR on 5×7 $p = 20$ mm AMC**	**SRR on 10×14 $p = 10$ mm AMC**	**SRR on 8×12 $p = 10$ mm AMC**	**SRR Antenna**
Size (mm × mm)	160 × 240	100 × 140	100 × 140	80 × 120	38 × 78
Resonant Frequency (MHz)	442 (440)	444 (454)	443 (456)	445 (458)	443 (443)
−10 dB Fractional Bandwidth (%)	2.11 (0)	3.58 (0.49)	2.01 (1.62)	1.46 (1.05)	0.95 (0.27)
Realized Gain (dBi)	1.5 (0.4)	−1.5 (−0.2)	−1.1 (−0.5)	−2.2 (1.0)	−7.5 (−13.1)
Radiation Efficiency (%)	62	49	45	43	24

mounted on the 8 by 12 20 mm periodicity surface reduced to −9 dB but remained at the same frequency. Evidently, the smaller AMC surfaces were not capable of attenuating surface waves to the same extent as the larger AMC surface. Therefore, when placed over a ground plane, the antennas mounted over the smaller AMC surfaces suffered from more edge effects which caused the ground plane to load the antenna. If a combined antenna/AMC structure were to be intentionally designed for use over a ground plane, the matching network could be adjusted to account for any loading by the ground plane.

The normalized radiation patterns of the antenna itself and the antenna combined with the AMCs are compared in Fig. 12. Principle E plane (y-z plane) and H plane (x-z plane) are shown on the left and right, respectively. In free space, the split ring antenna has dipole-like radiation patterns, omnidirectional in the H-plane and a figure of eight in the E-plane. However, when the SRR was placed on a ground plane its radiation pattern became asymmetrical in both planes, and its realized gain dropped by roughly 6 dB in the boresight direction. This was because close to the metal plate the

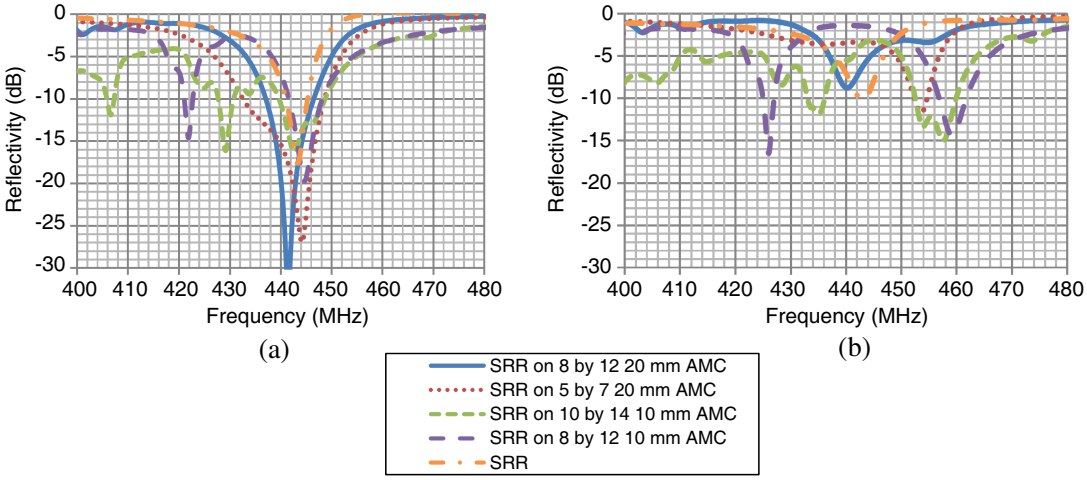

Figure 11. Measured reflectivity of AMC mounted SRR (a) in free space and (b) over a ground plane.

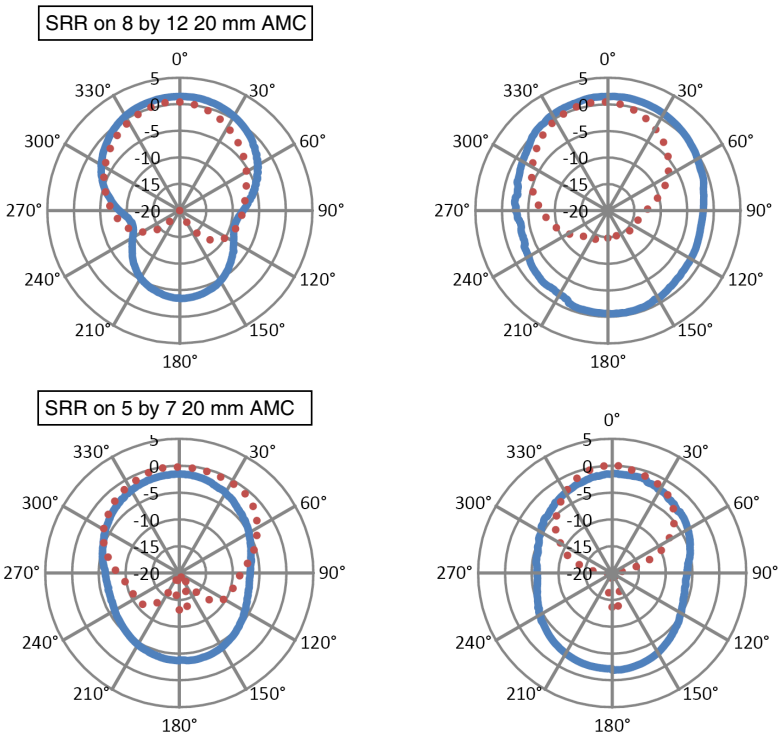

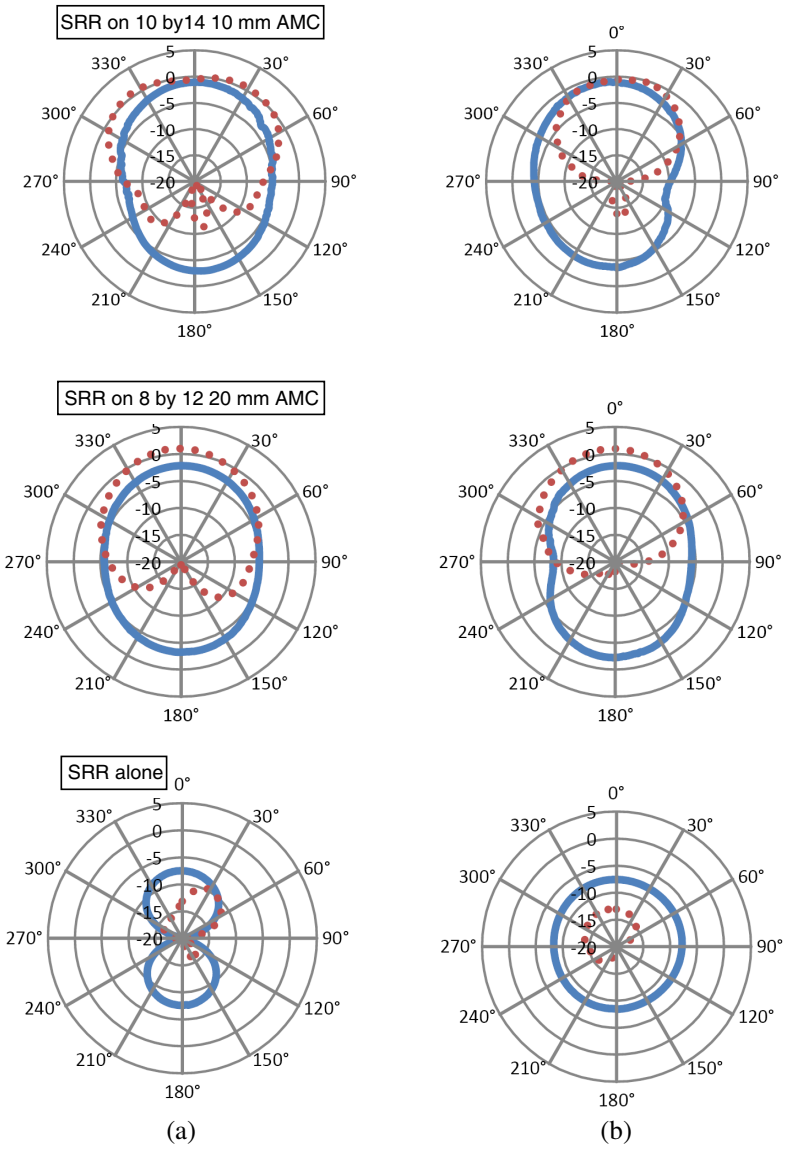

Figure 12. Measured radiation patterns in (a) E plane and (b) H plane of AMC mounted SRR in free space (solid) and over a ground plane (dashed) at frequency of maximum gain.

SRR and its image current cancelled out and consequently the resulting far-field radiation diminished. In contrast, the forward facing radiation lobes of the antennas which were mounted above an AMC surface did not suffer when the structure was moved from free space onto a metal plate. In fact, in most cases, the realized gain increased by 1 to 3 dB in the boresight direction, while the backward radiation was reduced by roughly 10 dB. The AMC therefore was clearly acting as a platform tolerant surface.

The measured realized gain level against frequency is shown in Fig. 13. It can be seen that for the antenna mounted above the largest AMC, the realized gain as a function of frequency remained relatively the same when the structure was moved from free space on to a metal plate. The peak measured gain of the antennas mounted above the smaller AMCs was seen to increase by up to 3 dB and occured 10 MHz higher in frequency when they were placed above a ground plane. The smaller AMCs cannot completely isolate the antenna from the effects of the surface on to which it is mounted. However, since the only observed potentially negative change in performance was a 10 MHz shift in operating frequency, the small AMC mounted antennas may prove an acceptable solution for applications in which space is limited, and the antenna will remain fixed above a ground plane.

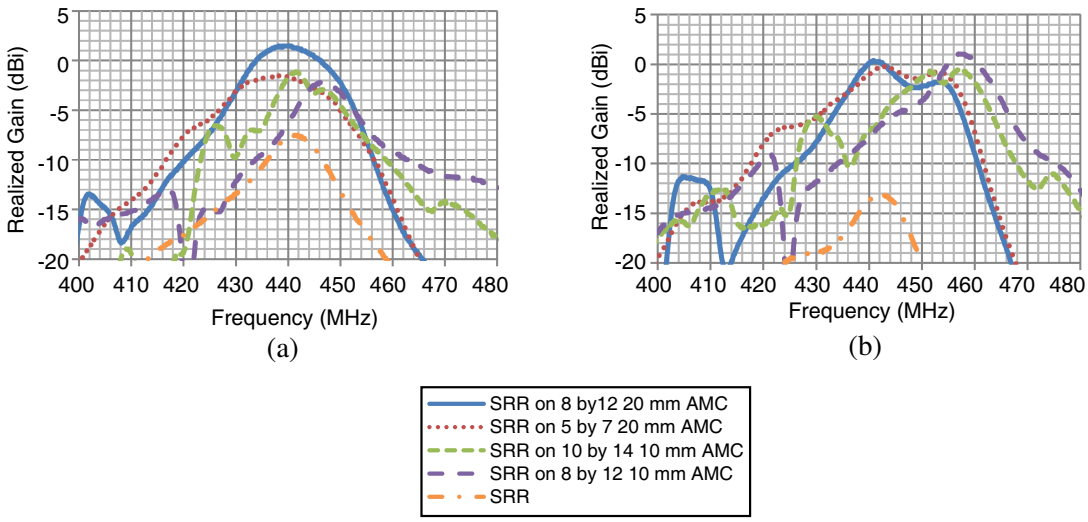

Figure 13. Measured realized gain of AMC mounted SRR (a) in free space and (b) over a ground plane.

5. CONCLUSION

An electrically small SRR antenna with loaded lumped elements was designed in this study. The antenna has a low profile, is low cost and can be easily integrated into the AMC system. Miniaturised AMC surfaces were also developed by using simple mushroom-like patches. By introducing capacitive loading, the unit cell size can be significantly reduced. By integrating the antenna with the AMC surface, the antenna performance can be significantly improved. It is found that without vias the AMC surface can only be miniaturized to a certain limit, but with vias the AMC periodicity can be reduced to a minimum scale of $\lambda/70$. An 8×12 array of 10 mm unit cell AMC ($ka = 0.53$) measuring ($0.11\lambda \times 0.17\lambda \times 0.019\lambda$) can provide a fractional bandwidth of 1.5% and 8.5 dB gain enhancement of the antenna. Aside from a reduced back lobe, the performance of the antenna that was mounted over the 20 mm 8×12 AMC array was relatively unchanged when the structure was moved from free space onto a metal surface and hence worked well as a platform tolerant antenna. The presence of the smaller AMC however did not make the antenna's performance completely independent of the platform on which it was mounted. Based on the user's requirements, a trade-off can be made between the detriment to the antenna's performance when placed over a metal ground plane and the overall size of the combined antenna and AMC structure.

ACKNOWLEDGMENT

Many thanks to the UK EPSRC for funding this study under grant EP/F067968.

REFERENCES

1. Chu, L. J., "Physical limitations of omni-directional antennas," *J. Appl. Phys.,* Vol. 19, 1163–1175, Dec. 1948.
2. Harrington, R. F., "Effect of antenna size on gain, bandwidth, and efficiency," *J. Res. National Bureau Standards — D. Radio Propagation,* Vol. 64D, No. 1, Jan. 1960.
3. McLean, J. S., "A re-examination of the fundamental limits on the radiation Q of electrically small antennas," *IEEE Transactions on Antennas and Propagation,* Vol. 44, No. 5, 672–676, May 1996.
4. Psychoudakis, D., J. L. Volakis, Z. N. Wing, S. K. Pillai, and J. W. Halloran, "Enhancing UHF antenna functionality through dielectric inclusions and texturization," *IEEE Transactions on Antennas and Propagation*, Vol. 54, No. 2, 317–329, Feb. 2006.

5. Lee, M., B. A. Kramer, C. Chen, and J. L. Volakis, "Distributed lumped loads and lossy transmission line model for wideband spiral antenna miniaturization and characterization," *IEEE Transactions on Antennas and Propagation*, Vol. 55, No. 10, 2671–2678, Oct. 2007.
6. Chi, P., R. Waterhouse, and T. Itoh, "Antenna miniaturization using slow wave enhancement factor from loaded transmission line," *IEEE Transactions on Antennas and Propagation,* Vol. 59, No. 1, 48–57, Jan. 2011.
7. Azadegan, R. and K. Sarabandi, "Bandwidth enhancement of miniaturized slot antennas using folded, complementary, and self-complementary realizations," *IEEE Transactions on Antennas and Propagation,* Vol. 55, No. 9, 2435–2444, Sep. 2007.
8. Erentok, A. and R. Ziolkowski, "Metamaterial-inspired efficient electrically small antennas," *IEEE Transactions on Antennas and Propagation,* Vol. 56, No. 3, 691–707, Mar. 2008.
9. Jin, P. and R. Ziolkowski, "Broadband, efficient, electrically small metamaterial-inspired antennas facilitated by active near-field resonant parasitic elements," *IEEE Transactions on Antennas and Propagation,* Vol. 58, No. 2, 318–327, Feb. 2010.
10. Ziolkowski, R., "Efficient electrically small antenna facilitated by a near-field resonant parasitic," *IEEE Antennas and Wireless Propagation Letters,* Vol. 7, 581–584, 2008.
11. Bilotti, F., A. Alu, and L. Vegni, "Design of miniaturized metamaterial patch antennas with μ-negative loading," *IEEE Transactions on Antennas and Propagation,* Vol. 56, No. 6, 1640–1647, Jun. 2008.
12. Qureshi, F., M. Antoniades, and G. V. Eleftheriades, "A compact and low-profile metamaterial ring antenna with vertical polarization," *IEEE Antennas and Wireless Propagation Letters,* Vol. 4, 333–336, 2005.
13. Liu, Q., P. S. Hall, and A. L. Borja, "Efficiency of electrically small dipole antennas loaded with left-handed transmission lines," *IEEE Transactions on Antennas and Propagation,* Vol. 57, No. 10, 3009–3017, Oct. 2009.
14. Lai, A. and T. Itoh, "Composite right/left-handed transmission line metamaterials," *IEEE Microwave Magazine,* 34–50, Sep. 2004.
15. Caloz, C., T. Itoh, and A. Rennings, "CRLH metamaterial leaky-wave and resonant antennas," *IEEE Antennas and Propagation Magazine,* Vol. 50, No. 5, 25–38, Oct. 2008.
16. Sievenpiper, D., L. Zhang, R. F. Jimenez Broas, N. G. Alexopolous, and E. Yablonovitch, "High-impedance electromagnetic surfaces with a forbidden frequency band," *IEEE Transactions on Microwave Theory and Techniques,* Vol. 47, No. 11, 2059–2074, Nov. 1999.
17. Folayan, O. and R. J. Langley, "Wideband reduced size electromagnetic bandgap structure," *IET Electronics Letters*, Vol. 41, 1099–1100, Sep. 2005.
18. Foroozesh, A. and L. Shafai, "Investigation into the application of AMCs to bandwidth broadening, gain enhancement and beam shaping of low profile and conventional monopole antennas," *IEEE Transactions on Antennas and Propagation,* Vol. 59, No. 1, 4–20, Jan. 2011.
19. Cook, B. S. and A. Shamim, "Utilizing wideband AMC structures for high-gain inkjet-printed antennas on lossy paper substrate," *IEEE Antennas and Wireless Propagation Letters*, Vol. 12, 76–79, 2013.
20. Liu, H., K. L. Ford, and R. J. Langley, "Miniaturised artificial magnetic conductor design using lumped reactive components," *IET Electronics Letters*, Vol. 45, No. 6, 294–295, 2009.
21. Liu, H., K. L. Ford, and R. J. Langley, "Design methodology for a miniaturized frequency selective surface using lumped reactive components," *IEEE Transactions on Antennas and Propagation*, Vol. 57, No. 9, 2732–2738, Sep. 2009.
22. Pendry, J. B., A. J. Holden, D. J. Robbins, and W. J. Stewart, "Magnetism from conductors and enhanced nonlinear phenomena," *IEEE Transactions on Microwave Theory and Technology*, Vol. 47, No. 11, 2075–2084, Nov. 1999.
23. Bilotti, F., A. Toscano, and L. Vegni, "Design of spiral and multiple SRRs for the realization of miniaturized metamaterial samples," *IEEE Transactions on Antennas and Propagation,* Vol. 55, No. 8, 2258–2267, Aug. 2007.

24. Martin, F., J. Bonache, F. Falcone, M. Sorolla, and R. Marques, "Split-Ring Resonator-based left-handed coplanar waveguide," *Applied Physics Letters*, Vol. 83, No. 22, Dec. 1, 2003.
25. Costa, F., O. Luukkonen, C. R. Simovski, A. Monorchio, S. A. Tretyakov, and P. M. de Maagt, "TE surface wave resonances on high impedance surface based antennas: Analysis and modeling," *IEEE Transactions on Antennas and Propagation*, Vol. 59, No. 10, 3588–3596, Oct. 2011.
26. Zhu, N. and R. Ziolkowski, "Active metamaterial-inspired broad-bandwidth, efficient, electrically small antennas," *IEEE Antennas and Wireless Propagation Letters*, Vol. 10, 1582–1585, 2011.
27. Ziolkowski, R., P. Jin, J. A. Nielsen, M. H. Tanielian, and C. L. Holloway, "Experimental verification of Z antennas at UHF frequencies," *IEEE Antennas and Wireless Propagation Letters*, Vol. 8, 1329–1333, 2009.
28. Zhu, N. and R. Ziolkowski, "Design and measurements of an electrically small, broad bandwidth, non-Foster circuit-augmented protractor antenna," *Applied Physics Letters*, Vol. 101, No. 2, 24107–24110, Jul. 2012.
29. Jin, P. and R. Ziolkowski, "Low-Q, electrically small, efficient near-field resonant parasitic antennas," *IEEE Transactions on Antennas and Propagation*, Vol. 57, No. 9, 2548–2563, Sep. 2009.
30. Vasundara, V. V., H. Wang, I. K. Kim, and S. Weiss, "SRR-loaded small dipole antenna with electromagnetic bandgap ground plane," *IEEE International Symposium on Antennas and Propagation 2011*, 1040–1043, Jul. 2011.
31. Best, S. R., "The radiation properties of electrically small folded helix antennas," *IEEE Transactions on Antennas and Propagation*, Vol. 52, No. 4, 953–960, Apr. 2004.
32. Johnston, R. H. and J. G. McRory, "An improved small antenna radiation-efficiency measurement method," *IEEE Antenna and Propagation Magazine,* Vol. 40, No. 5, 40–48, Oct. 1998.